RSC Advances

PAPER

View Article Online
View Journal | View Issue

Cite this: *RSC Adv.*, 2017, **7**, 41880

Effect of Nb doping in WO_3/ZrO_2 catalysts on gas phase dehydration of glycerol to form acrolein†

Ku-Hsiang Sung and Soofin Cheng *

Gas-phase dehydration of glycerol to produce acrolein was investigated over tungstated zirconia catalysts with and without niobium doping, in order to correlate the catalytic activity and life-stability with the acid/base properties of the catalysts. The results of NH_3- and CO_2-TPD experiments showed that the tungstated zirconia catalysts contained both acidic and basic sites, and the amounts decreased with the increase in calcination temperature. The most suitable calcination temperature for 20% WO_3/ZrO_2 as the catalyst in the gas phase dehydration of glycerol to form acrolein was 450 °C in consideration of achieving high acrolein yield and long lifetime of the catalyst. Not only the amount of acid but also the amount of base affected the acrolein yield. Doping a small amount of niobium further increased the life-stability of the catalysts, attributed to the decrease in the number of basic sites. The influence of Nb is mostly in neutralization of surface acidity electronically instead of geometric blocking of the basic sites. Moreover, fine tuning the ratio of acid/base sites was found to be important in achieving good catalytic performance in the gas-phase dehydration of glycerol to generate acrolein. The ratio of acid/base sites in the range of 4–5.4 gave the highest glycerol conversion, and acrolein yield and lowest catalyst decay rate. The spent catalysts were easily regenerated by calcination at 450 °C, and the catalytic activities were retained well even after the second time of reuse.

Received 24th July 2017
Accepted 22nd August 2017

DOI: 10.1039/c7ra08154e

rsc.li/rsc-advances

1. Introduction

To decrease the global demand for fossil fuels and reduce CO_2 emission, there has been great interest in producing fuels and chemicals from renewable feedstock. Biodiesel is considered one of the best choices among several alternative fuels because of its CO_2-neutral production and slight impact on engine performance.[1] Biodiesel is currently synthesized by base-catalyzed transesterification of triglyceride with short chain alcohols on a large scale, accompanied by the formation of 10 wt% of glycerol as byproduct.[2] Although political regulations have pushed the production of biofuels in order to fulfill the CO_2 reduction objectives fixed by the Kyoto climate protocol and lately the Paris Agreement, it is not yet possible to produce any of these biofuels as economical competitors to fossil fuels. One of the possible ways to reduce the production cost of biodiesel is using glycerol to produce value-added chemicals. When considering a commercial target, the catalytic dehydration of glycerol to acrolein is the most promising route for valorizing glycerol because acrolein has many applications in industrial processes, such as the precursors of acrylic acid and biocides.[3]

Dehydration of glycerol to form acrolein has been exercised since 1930, Schering-Kahlbaum claimed the first patent of acrolein production from glycerol in gas-phase over lithium phosphate supported on pumice stone.[4] The rate of acrolein decomposition was found to be faster than that of acrolein formation in the absence of acid catalyst. Since then, sulfuric acid was used as the catalyst in liquid phase dehydration of glycerol.[5,6] However, corrosion hazard and difficulties in handling and product separation are the drawbacks. Although solid acid catalysts such as clay and alumina supported phosphoric acid[7,8] and heteropolyacids[9,10] were effective as the dehydration catalysts in liquid phase, it is still hazardous to operate the reaction under supercritical water pressure.

Gas-phase dehydration of glycerol to produce acrolein has been promoted by solid acids. Dubois *et al.*[11,12] studied the catalytic performances of various solid acids, including zeolites, Nafion and WO_3/ZrO_2, in gas-phase dehydration of glycerol, and concluded that solid acids with Hammett acidities (HAs) in the range of −10 to −16 were suitable catalysts. They also reported for the first time that WO_3/ZrO_2 had high activity in catalyzing gas-phase dehydration of glycerol to produce acrolein. In 2007, Chai *et al.*[13] examined a large group of solid materials including zeolites, SAPOs, metal oxides, supported phosphoric and heteropoly acids, and sulfated and tungstated zirconia, in catalyzing gas-phase dehydration of glycerol. They concluded that solids with HAs in the range of −3 to −8.2 were most active catalysts in generating acrolein. Among the solids, 15 wt% WO_3/ZrO_2 showed

Department of Chemistry, National Taiwan University, Roosevelt Rd. Sec. 4, Taipei 106, Taiwan. E-mail: chem1031@ntu.edu.tw; Fax: +886-2-33668671

† Electronic supplementary information (ESI) available: TPD-NH_3 and CO_2, TG profiles and catalyst reusability. See DOI: 10.1039/c7ra08154e

the highest glycerol conversion and acrolein selectivity. Nevertheless, deactivation of the catalysts with time-on-stream (TOS) was the main concerns. In 2011, Ulgen *et al.*[14] reported the use of WO_3/TiO_2 instead of WO_3/ZrO_2 as the catalyst in gas-phase dehydration of glycerol, and they found that co-feeding of oxygen could reduce deactivation rate of the catalyst.

Niobium based catalysts have been tested in dehydration of glycerol to form acrolein.[15–20] Chai *et al.*[15] reported that the niobia calcined at 400 °C gave the highest glycerol conversion and acrolein selectivity. Shiju *et al.*[16] studied silica supported niobia catalysts and found that the glycerol conversion and acrolein selectivity depended on the niobia loading and calcination temperature. However, in both aforementioned works, the niobia catalysts showed glycerol conversions decreased rapidly with TOS. Lauriol-Garbey *et al.*[19,20] used zirconium and niobium mixed oxides (ZrNbO) as catalysts for glycerol dehydration. The ZrNbO catalysts gave the recorded high conversion of 82% even after 177 h on stream with acrolein selectivity remaining 72%. However, these results have not been repeated by other research groups. Lately, the same group reported SiO_2-doped WO_3/ZrO_2 as catalysts in dehydration of glycerol.[21] However, the catalytic lifetime was much shorter than that of ZrNbO. Recently, niobium species supported on a zirconium doped porous silica were used as the catalysts, but acrolein selectivity of 45 mol% was obtained after 2 h TOS.[22] In the present study, we disclosed a novel finding that doping a small amount of niobium to WO_3/ZrO_2 catalysts would increase the life-stability of the catalysts. Moreover, relatively high acrolein selectivities (*ca.* 70%) could be retained. Efforts were put in correlation of the active sites with the decay rate of the catalysts.

2. Experimental methods

2.1 Catalyst synthesis

Tungstated zirconia was prepared by wet impregnation method. For the WO_3/ZrO_2 catalyst of 20% weight ratio, a solution containing 0.2656 g $(NH_4)_6H_2W_{12}O_{40}\cdot xH_2O$ dissolved in 5 mL deionized water was added dropwise onto 1.2926 g $Zr(OH)_4$ powders under static condition, and the mixture was left steady for 1 h before the solvent was removed by rotary evaporation.[23,24] After drying at 100 °C overnight, the powders were calcined in air at temperatures in the range of 400 to 800 °C for 3 h with a ramping rate of 1 °C min^{-1}. The niobium doped tungstated zirconia catalysts were prepared by the procedures similar to the foregoing method, except proper amounts of niobium oxalate were added in the solution of ammonium metatungstate hydrate for impregnation on $Zr(OH)_4$ powders. After drying at 100 °C overnight, the powders were calcined at 450 °C for 3 h in air. The resultant materials were designated as *X*-$NbWO_x/ZrO_2$-450, where the WO_3/ZrO_2 weight ratios were kept at 20%, and *X* varied in 1, 3, and 5% is the $Nb_2O_5/(WO_3 + ZrO_2)$ weight ratio.

2.2 Catalyst characterization

Powder X-ray diffraction (PXRD) patterns were recorded with a Panalytical X'Pert diffractometer using Cu Kα radiation in an operating mode of 45 kV and 40 mA. Nitrogen physisorption was carried out in a Micromeritics TriStar 3000 system. Prior to the physisorption, the sample was degassed at 200 °C under 10^{-3} torr for at least 8 h. Acidity and basicity of the catalysts were determined by temperature-programmed desorption of NH_3 and CO_2, respectively, using an AutoChem 2910 system with a TCD detector. About 0.25 gram of the sample was heated in a 50 mL min^{-1} of He flow at calcination temperature for 1 h to remove the adsorbed moisture. Then, 5% ammonia in He or pure CO_2 gas (50 mL min^{-1}) was passed through the sample at 100 °C for 1 h, followed by purging the sample with pure He (30 mL min^{-1}) for another hour. The TCD signals of the effluent were recorded when the sample was heated from 100 to 600 °C with a ramping rate of 10 °C min^{-1}. FTIR spectra were conducted using a Nicolet Magna FT-IR 550 spectrometer. The resolution of the recorded spectra is 4 cm^{-1}. 25 mg of the sample was pressed into a disk and placed inside the cell. After heated at 450 °C under 10^{-4} torr for 1 h and cooled down to room temperature, the sample was exposed to pyridine vapor for 30 min and evacuated to 10^{-4} torr for another 30 min to remove pyridine vapor in the gas phase. The IR spectra were recorded under 10^{-4} torr while the temperature was raised to 400 °C at 100 °C intervals. Scanning electron microscopy (SEM) photographs were taken using a Hitachi S-4800 Field Emission Scanning Electron Microscope.

2.3 Catalytic reaction

Gas-phase dehydration of glycerol was carried out at 290 °C under ambient pressure in a vertical fixed-bed tubular quartz reactor. The catalyst (300 mg) in fine powders was mixed with quartz (300 mg) and then sandwiched in the middle of the reactor with quartz wool. Prior to the reaction, the catalyst was pretreated at 290 °C for 1 h under flowing dry nitrogen (60 mL min^{-1}). An aqueous solution of 10 wt% glycerol was fed into the reactor by a syringe pump with a flow rate of 8 mL h^{-1}. The products were collected hourly by an ice-water trap and analyzed by a gas-chromatography (GC) equipped with a capillary column (BP-20) and a FID detector. The glycerol conversion and selectivities of identified products were calculated according to the following equations:

$$\text{Conversion (\%)} = (\text{initial mol} - \text{final mol})\ \text{of glycerol}/\ \text{initial mol of glycerol} \times 100\% \quad (1)$$

$$\text{Selectivity (\%)} = (\text{specific product in mol})/\ (\text{initial mol} - \text{final mol})\ \text{of glycerol} \times 100\% \quad (2)$$

3. Results and discussion

3.1 Effect of calcination on WO_3/ZrO_2 catalysts

3.1.1 Characterization. XRD patterns of the WO_3/ZrO_2 catalysts show that calcined at 400 °C to be amorphous (Fig. 1). As the calcination temperature increases, the peaks of the tetragonal ZrO_2 (2θ = 30.3, 34.4, 50.3 and 60.0°) start to show and grow with temperature. At calcination temperature of 800 °C, monoclinic ZrO_2 (characteristic peaks at 2θ = 28.2 and 31.5°) appears. Meanwhile, the monoclinic WO_3 phase (2θ =

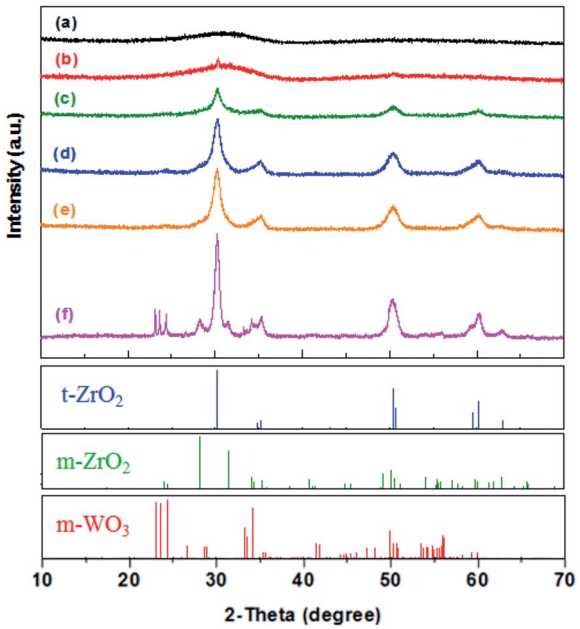

Fig. 1 XRD patterns for WO_3/ZrO_2 catalysts calcined at: (a) 400, (b) 450, (c) 500, (d) 600, (e) 700 and (f) 800 °C, in comparison to the JCPDS patterns of tetragonal and monoclinic ZrO_2 and monoclinic WO_3.

Table 1 Textural properties of WO_3/ZrO_2 catalysts calcined at different temperatures and those doped with Nb

Sample	S_{BET} ($m^2\ g^{-1}$)	Pore diameter[a] (nm)	Pore volume ($cm^3\ g^{-1}$)
WO_3/ZrO_2-400	254	3.7	0.241
WO_3/ZrO_2-450	223	4.4	0.222
WO_3/ZrO_2-500	189	5.1	0.248
WO_3/ZrO_2-600	138	5.3	0.221
WO_3/ZrO_2-700	134	6.3	0.239
WO_3/ZrO_2-800	62	12	0.224
1% $NbWO_x/ZrO_2$-450	233	5.0	0.278
3% $NbWO_x/ZrO_2$-450	236	5.3	0.302
5% $NbWO_x/ZrO_2$-450	242	5.6	0.302

[a] Determined by BJH method at peak maximum of pore size distribution profile.

23.2, 23.6 and 24.4°) is also detected, suggesting that the crystalline WO_3 is formed and dispersed on the ZrO_2 support.

Nitrogen sorption isotherms of the calcined WO_3/ZrO_2 catalysts show type IV isotherms with the hysteresis loops appeared at p/p_0 of 0.5–0.9, implying that these materials own mesopores. The derived textural properties are given in Table 1. A decrease in surface area and increase in pore diameter are observed with increasing the calcination temperature, and both are originated from sintering of the metal oxide particles at high temperatures.

NH_3- and CO_2-TPD experiments were used to measure the surface concentrations of acidic and basic sites, respectively. Fig. S1(A) (ESI†) shows that the total acid amounts of the WO_3/ZrO_2 catalysts measured by NH_3-TPD decrease with calcination temperature, and the desorption peaks appear mainly in the range of 150–500 °C. These results are in consistence with that reported by García-Sancho *et al.*[25] that the acidic strengths of the WO_3/ZrO_2 catalysts were in the range of weak to moderate. However, it is noticed that the sample calcined at 400 °C have additional desorption peaks at temperatures above 400 °C. The high temperature peak decreases in intensity and shifts to temperatures above 470 °C for the sample calcined at 450 °C.

Fig. S1(B) (ESI†) compares the base amounts of WO_3/ZrO_2 catalysts calcined at different temperatures measured by CO_2-TPD experiment. Again, the total base amounts of the WO_3/ZrO_2 catalysts decrease with the calcination temperature. Three peak maxima can be seen at *ca.* 190, 380 and 530 °C on the sample calcined at 400 °C. The last high temperature peak is hardly seen on the sample calcined at 450 °C. In combination of the CO_2-TPD and NH_3-TPD results, it can be concluded that most of the surface hydroxyl groups condensate in the temperature range of 400–450 °C. Moreover, the high temperature peak observed on the NH_3-TPD profile of WO_3/ZrO_2 calcined at 450 °C should not be due to condensation of surface hydroxyl groups. Instead, it corresponds to some strong acidic sites present on the sample.

Table 2 summarizes the acid and base densities based on the desorption peak areas of NH_3-TPD and CO_2-TPD, respectively, of WO_3/ZrO_2 calcined at different temperatures. It is noticed that those calcined at 400–600 °C have acid densities in a close range of 0.145–0.165 sites per nm^2, while those calcined at 700 and 800 °C have slightly lower and higher acid density of 0.130 and 0.183 sites per nm^2, respectively. On the other hand, base densities decrease almost linearly with the increase of calcination temperature. As the surface area decreases with calcination temperature, Fig. 2 shows that the acid and base densities as a function of surface area varied in the reverse trend. Base density increases with surface area, while acid density decreases with surface area but merely in a narrow range. These results infer that the amount of basic sites increases more abruptly than that of acid sites with the increase of surface area, and the latter is almost linearly proportional to the surface area.

3.1.2 Catalytic performance of WO_3/ZrO_2 calcined at different temperatures. Fig. 3 shows the results of gas phase dehydration of glycerol catalyzed by WO_3/ZrO_2 calcined at different temperatures. The glycerol conversions are all nearly 100% at the beginning, and then they decay with time on stream. Moreover, the decay rate is faster for the catalyst calcined at higher temperatures (Fig. 3A). On the other hand, the acrolein selectivities vary in similar trends with time-on-stream over all WO_3/ZrO_2 catalysts calcined at different temperatures (Fig. 3B). The acrolein selectivities increase in the first two hours and become steady with time on stream. The low acrolein selectivities in the first hour may be due to that the system is not in dynamic stability. Other researchers also reported lower than 90% calculated carbon balance in the initial reaction time.[14,26] The conversions and products distribution in 3–4 h and those in 11–12 h are tabulated in Table 3. Acrolein is the major product, while hydroxylacetone (HA), acetaldehyde (AD), and allyl alcohol (AA) are minor products. Moreover, there are *ca.* 20 mol% of carbon

Table 2 Results of NH_3-TPD and CO_2-TPD measurements on WO_3/ZrO_2 catalysts calcined at different temperatures

Catalyst	Acid amount (10^{18} g^{-1})	Acid density (nm^{-2})	Base amount (10^{18} g^{-1})	Base density (nm^{-2})	Decay rate[b] (%/h)
WO_3/ZrO_2-400	36.8	0.145	15.1	0.0595	−0.32[c]
WO_3/ZrO_2-450	32.6 (2.9)[a]	0.146 (0.013)[a]	11.4	0.0510	−0.39[c]/−1.37[e]
WO_3/ZrO_2-500	31.2	0.165	8.10	0.0430	−0.70[d]
WO_3/ZrO_2-600	22.8	0.165	6.81	0.0494	−2.00[d]
WO_3/ZrO_2-700	17.4	0.130	5.20	0.0388	−7.50[d]
WO_3/ZrO_2-800	11.3	0.183	1.73	0.0279	−9.50[d]
1% $NbWO_x/ZrO_2$-450	30.3 (3.3)	0.130 (0.014)	8.46	0.0363	−0.37[e]
3% $NbWO_x/ZrO_2$-450	33.7 (3.3)	0.143 (0.014)	7.84	0.0332	−0.14[e]
5% $NbWO_x/ZrO_2$-450	34.8 (5.3)	0.144 (0.022)	7.57	0.0313	−0.63[e]

[a] Values in parenthesis are strong acid sites (>500 °C on NH_3-TPD profiles). [b] From the slopes of glycerol conversions *vs.* TOS based on TOS. [c] From the slopes of glycerol conversions *vs.* TOS based on TOS in 3–9 h. [d] From the slopes of glycerol conversions *vs.* TOS based on TOS 3–6 h in Fig. 3A. [e] From the slopes of glycerol conversions *vs.* TOS based on TOS 7–12 h in Fig. 5A.

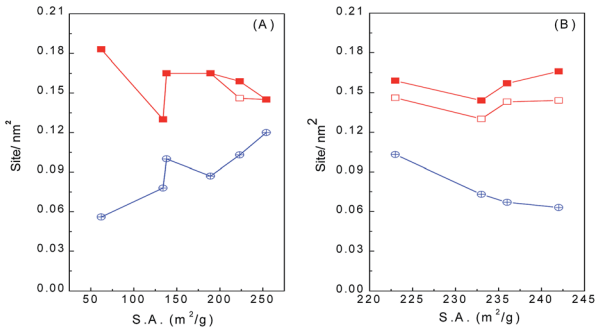

Fig. 2 Correlation of acid/base densities with the surface areas of (A) WO_3/ZrO_2 calcined at different temperatures, and (B) WO_3/ZrO_2-450 doped with various amounts of Nb; (■) total acid, (□) weak acid, (⊕) base.

imbalance, which are shown as "Unknowns". Since all the used catalysts turn black, it is assumed that the Unknowns are coke and polymeric materials.

Dalil's group has confirmed the coke formation at initial stage of gas phase glycerol dehydration, and the amount of coke deposited on WO_3/TiO_2 catalysts was found to increase with TOS.[27–29] Since the selectivities of Unknowns over our catalysts are quite steady as a function of TOS (3–4 h *vs.* 11–12 h in Table 3). It is also consistent with the finding by Dalil's group.

In comparison of WO_3/ZrO_2 calcined at different temperatures, those calcined at 450–700 °C give relatively higher acrolein selectivities of 68–71% (Fig. 1 and Table 3). Moreover, acrolein selectivities retain almost unchanged with TOS for catalysts calcined at 450–600 °C. For the catalyst calcined at lowest temperature, WO_3/ZrO_2-400, which contains the largest amounts of both acidic and basic sites, is most stable on TOS. However, the acrolein selectivity is among the lowest. In contrast, WO_3/ZrO_2 calcined at highest temperatures, WO_3/ZrO_2-700 and -800, have very fast decay rates and larger amounts of coke formation. Judging by the stabilities of the catalysts and high acrolein selectivities, the most suitable calcination temperature for $WO_3/$

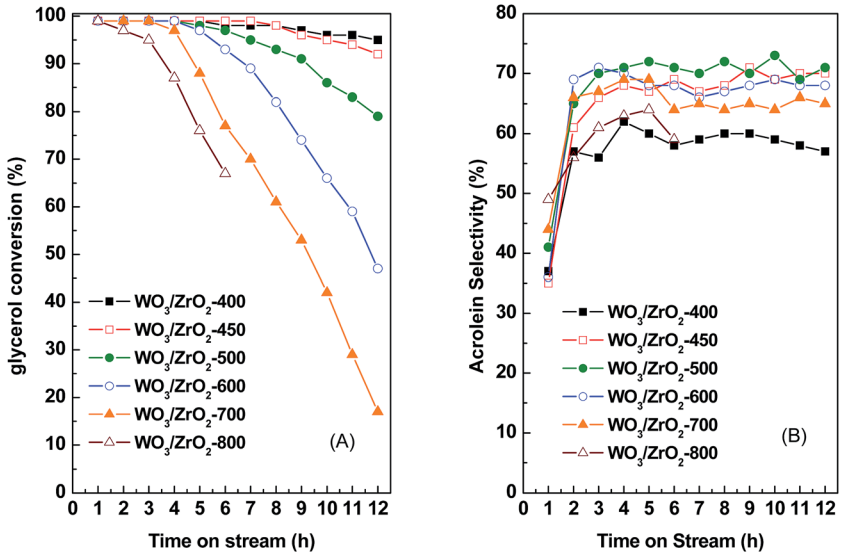

Fig. 3 Evolution of (A) glycerol conversion and (B) acrolein selectivity as a function of time on stream at 290 °C for the WO_3/ZrO_2 catalysts calcined at different temperatures. 0.3 g catalyst, GHSV = 1117 h^{-1}, 60 mL min^{-1} N_2 flow rate.

Table 3 Product distributions in glycerol dehydration over WO_3/ZrO_2 catalysts calcined at different temperatures[a]

		Product selectivity (%)				
Catalysts	Conversion (%)	Acrolein	AD	AA	HA	Unknowns
WO_3/ZrO_2-400	99 (95)	62 (57)	6 (4)	2 (1)	9 (18)	21 (20)
WO_3/ZrO_2-450	99 (92)	68 (70)	6 (4)	1 (2)	9 (12)	16 (12)
WO_3/ZrO_2-500	99 (79)	71 (71)	6 (5)	2 (3)	4 (9)	17 (12)
WO_3/ZrO_2-600	99 (47)	70 (68)	4 (3)	2 (3)	7 (8)	17 (18)
WO_3/ZrO_2-700	97 (17)	69 (65)	2 (1)	2 (3)	4 (6)	23 (25)
WO_3/ZrO_2-800	87	63	1	1	6	29

[a] Reaction conditions: 290 °C, 0.3 g catalyst, GHSV = 1117 h^{-1}, 60 mL min^{-1} N_2 flow rate. AD = acetaldehyde; AA = allyl alcohol; HA = 1-hydroxylacetone. Selectivity for unknowns = (100 − known products)%. The selectivity data were obtained at TOS = 3–4 h, and those in parenthesis obtained at TOS = 11–12 h of reaction.

ZrO_2 catalyst is 450 °C. Therefore, the catalysts studied hereafter were calcined at 450 °C.

3.2 WO_3/ZrO_2 catalysts doping with niobium

3.2.1 Characterization. The WO_3/ZrO_2 catalysts doping with 1–5% Nb_2O_5 show similar XRD patterns and nitrogen sorption isotherms as those of WO_3/ZrO_2-450. However, the surface area, pore diameter, and pore volume of the Nb-doped catalysts increase slightly in comparison to those of pristine WO_3/ZrO_2-450 (Table 1). These results infer that the incorporation of Nb(v) in WO_3/ZrO_2 probably helps the dispersion of WO_3 on ZrO_2.

Fig. S2 (ESI†) shows the SEM photographs of WO_3/ZrO_2-450 catalyst and those doped with 1% and 3% Nb_2O_5. All of them are aggregates of nanoparticles *ca.* 10 nm in diameter and hard to estimate the individual oxide particle size. It is apparent that the doping of 1–3 wt% Nb_2O_5 does not cause the drastic change of the morphology of WO_3/ZrO_2 oxides, and no particles of other morphologies can be seen. This result implies that Nb is probably distributed homogeneously in the oxides.

Fig. S3 (ESI†) shows the NH_3- and CO_2-TPD profiles of WO_3/ZrO_2-450 catalysts doped with different amounts of Nb_2O_5, in comparison with those of pristine WO_3/ZrO_2-450. Fig. S3(A) (ESI†) shows that all the samples have similar NH_3 desorption profiles: a broad band covering from 100 to 450 °C and a weak peak appeared above 450 °C. The possibility that the high temperature peaks are due to the condensation of surface hydroxyl groups can be excluded because they do not show in the CO_2-TPD profiles (Fig. S3(B), ESI†). Hence, the presence of the small high temperature peaks in NH_3-TPD profiles implies that the materials contain a small amount of strong acidic sites, probably attributed to formation of Nb_2O_5 clusters. Nevertheless, the majority of the acidic sites is in the weak to medium strength region. The intensities of the low temperature peaks decrease when only 1 wt% Nb_2O_5 is doped, and contrarily increase when it is further increased to 3 and 5% (Fig. S3(A), ESI†). However, the positions of desorption maxima retain at almost the same temperature around 200 °C, implying no significant change in acid strength of the catalysts with niobium doping.

The CO_2-TPD profiles in Fig. S3(B) (ESI†) show that the base amounts decrease markedly when as low as 1% Nb_2O_5 is doped on WO_3/ZrO_2-450. The decrease in base amount is attributed to that Nb would neutralize the basic sites present on the zirconia support.[15] However, the change in base amounts is less significant as the doping amount of Nb is further increased. The phenomenon can be explained by that the influence of Nb is mostly in neutralization of surface acidity electronically instead of geometrically blocking the basic sites. Moreover, Fig. S3(B)† shows that the basic sites of strongest strength with the CO_2 desorption peak appeared above 400 °C are suppressed completely, while those of weakest strength with the desorption peak appeared at 100–330 °C are partially suppressed and those around 380 °C are hardly affected by Nb-doping.

The acid and base densities estimated from the desorption peak areas of NH_3-TPD and CO_2-TPD of Nb-doped WO_3/ZrO_2-450 samples are also summarized in Table 2. The acid densities are almost unchanged (0.143–0.146 nm^{-2}), except the one doped with 1% Nb_2O_5 has lower value of 0.130 nm^{-2}, while the base density decreases from 0.0510 nm^{-2} to 0.0313–0.0363 nm^{-2} with Nb doping. Fig. 2B plots the acid/base densities on Nb-doped WO_3/ZrO_2-450 as a function of surface area. It clearly shows that the acid densities are constrained in a narrow range while the base densities decrease with the increase in surface areas.

The nature of the acidic sites was examined by taking the FT-IR spectra of the catalysts after pyridine adsorption. Fig. 4 compares the FT-IR spectra of WO_3/ZrO_2-450 and that doped with 3% Nb_2O_5. At the desorption temperature of 100 °C, both samples show a strong peak at 1445 cm^{-1} attributing to pyridine adsorbed on the Lewis acid sites and a weak peak at 1545 cm^{-1} attributing to pyridine adsorbed on the Brønsted acid sites. In addition, the peaks at 1575 and 1610 cm^{-1} correspond to pyridine adsorbed on the weak and strong Lewis acid sites, respectively. At the desorption temperature of 300 °C, the 1545 cm^{-1} peak disappears completely while the 1445 and 1610 cm^{-1} peaks still retain some intensity for both samples. These results imply that both Nb_2O_5-doped and undoped WO_3/ZrO_2-450 materials contain mainly the Lewis acidic sites, and the strength of Lewis acidic sites is stronger than that of Brønsted acid sites. Moreover, 3% $NbWO_3/ZrO_2$-450 contains slightly larger amount of strong Lewis acidic sites than WO_3/ZrO_2-450, judging by the peak intensities of the FT-IR spectra taken at desorption temperatures of 200–300 °C.

3.2.2 Catalytic performance of Nb-doped WO_3/ZrO_2. Fig. 5 shows the results of dehydration of glycerol catalyzed by Nb-

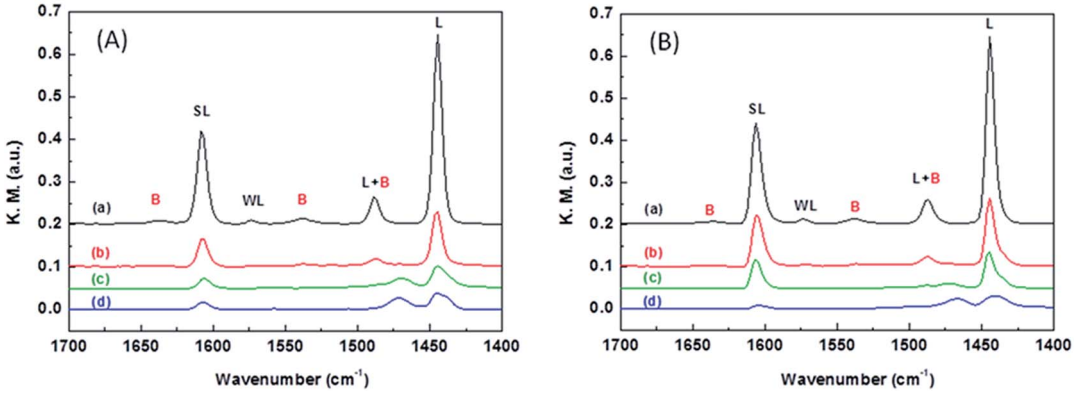

Fig. 4 FT-IR spectra of (A) WO_3/ZrO_2-450, (B) 3% $NbWO_x/ZrO_2$-450 after pyridine adsorption at various evacuation temperatures: (a) 100 °C (b) 200 °C (c) 300 °C (d) 400 °C.

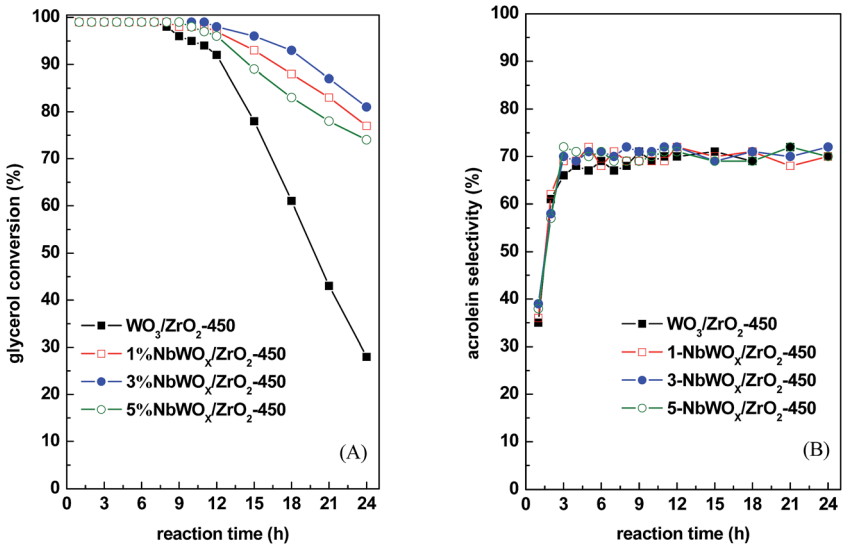

Fig. 5 Evolution of (A) glycerol conversion and (B) acrolein selectivity as a function of time on stream at 290 °C for the WO_3/ZrO_2-450 and $NbWO_x/ZrO_2$-450 catalysts with different Nb_2O_5 weight ratios to (WO_3 + ZrO_2). 0.3 g catalyst, GHSV = 1117 h^{-1}, 60 mL min^{-1} N_2 flow rate.

doped WO_3/ZrO_2-450, in comparison to that of pristine WO_3/ZrO_2-450. The decay in glycerol conversion upon TOS is markedly slowed down over the Nb-doped catalysts. Table 4 compares the conversions and product distributions in 3–4 h and those in 23–24 h. All the catalysts give nearly complete conversion in 3–4 h TOS, but that drastic decreases to 28% after 23–24 h TOS is seen over pristine WO_3/ZrO_2-450. In contrast, all the Nb-doped catalysts can retain relatively high conversions of 74–81% after 23–24 h TOS. The catalytic stabilities vary with the doping amounts of Nb_2O_5 in the order of 5% < 1% < 3%. Acrolein is the major product, and the acrolein selectivity is not changed with Nb-doping or TOS. It retains around 70% over all the catalysts. HA, AD, and AA are obtained as the minor products and their selectivities are not affected by Nb-doping, while the Unknowns decrease slightly with Nb-doping. The optimal catalytic performance was obtained over 3% $NbWO_x/ZrO_2$-450 with 81% glycerol conversion and 72% acrolein selectivity at 24 h TOS.

3.3 Reusability of catalyst

The reusability of 3% $NbWO_x/ZrO_2$-450 catalyst was examined. The spent catalyst after reaction at 290 °C for 24 h was regenerated by calcination at 450 °C for 3 h to burn the coke disposed on the surface of the catalyst. Fig. S4 (ESI†) showed the TG profile of the used 3% $NbWO_x/ZrO_2$-450 catalyst obtained in air. The coke deposition on the used catalyst is about 19 wt%. Moreover, the profile indicates that 17 wt% is burned away at temperature below 450 °C and only 2 wt% coke is still remained after calcination at 450 °C. Fig. S5 (ESI†) compares the catalytic performances of the fresh and regenerated 3% $NbWO_x/ZrO_2$-450 catalysts. The results showed that the glycerol conversion and selectivity to acrolein are well retained even the catalyst is regenerated and reused for second time. The similar variation patterns in glycerol conversions and acrolein selectivities as a function of TOS provide a solid evidence that the initial low acrolein selectivities are due to that the system is not in dynamic stability, instead of rapid coke formation as proposed by Dalil *et al.*[29] These results also infer that

Table 4 Product distributions in glycerol dehydration over WO_3/ZrO_2-450 with and without Nb_2O_5 doping[a]

		Product selectivity (%)				
Catalysts	Conversion (%)	Acrolein	AD	AA	HA	Unknowns
WO_3/ZrO_2-450	99 (28)	68 (70)	6 (6)	1 (3)	9 (15)	16 (6)
1% $NbWO_x/ZrO_2$-450	99 (77)	69 (70)	8 (5)	2 (2)	11 (14)	10 (9)
3% $NbWO_x/ZrO_2$-450	99 (81)	69 (72)	7 (5)	1 (2)	9 (15)	14 (6)
5% $NbWO_x/ZrO_2$-450	99 (74)	71 (70)	8 (5)	2 (3)	11 (17)	8 (5)

[a] Reaction conditions: 290 °C, 0.3 g catalyst, GHSV = 1117 h^{-1}, 60 mL min^{-1} N_2 flow rate. AD = acetaldehyde; AA = allyl alcohol; HA = 1-hydroxylacetone; selectivity for unknowns = (100 − known products)%. The selectivity data were data obtained at TOS = 3–4 h, and those in parenthesis obtained at TOS = 23–24 h of reaction.

2 wt% coke deposition on the 3% $NbWO_x/ZrO_2$-450 catalyst does not significantly vary the acid/base active sites and has negligible influence on the catalyst activity.

3.4 Catalytic active sites

Zirconia is considered to be one of the amphoteric oxides and contains both acidic and basic sites on its surface. Addition of WO_3 to zirconia was found to significantly decrease the amount of basic sites and slightly increase the acidic sites.[30] When used as the catalysts in gas-phase dehydration of glycerol, ZrO_2 gave complicated products with acetol (also known as hydroxylacetone, HA) as the largest portion of products (25% selectivity), while WO_3/ZrO_2 gave acrolein of 70% selectivity as the main product.[31] Kinage *et al.*[32] studies Na-doped metal oxides as the catalysts for glycerol conversion and proposed that the basic sites were responsible for HA formation. Chai *et al.*[13] suggested that the strong acidic sites of Hammett constant in −8.2 to −3.0 were more efficient than those of medium to weak acid sites in acrolein formation. Besides, Lewis acids such as Al_2O_3 and Nb_2O_5 showed lower acrolein selectivities (*ca.* 40 mol%) than the materials containing Brønsted acids, such as supported phosphoric acid and heteropoly acid (60–70 mol%). On the other hand, the polyglycerols or acetalization products of glycerol were considered to form and be adsorbed on basic sites.[33,34]

In our case, the glycerol consumption rate increases almost linearly with both amounts of acid and base sites, based on the

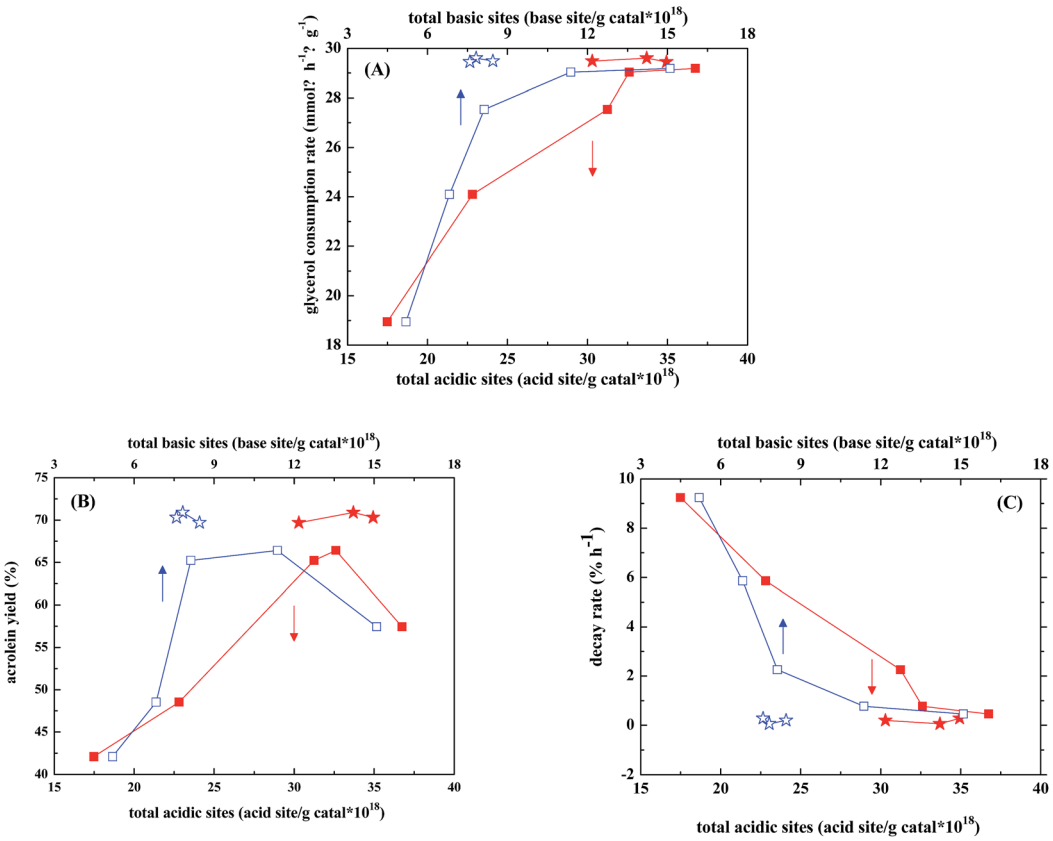

Fig. 6 Correlations of (A) specific glycerol consumption rates, (B) acrolein yields, and (C) decay rates (average in 3–12 h TOS) with total acidic/basic sites on WO_3/ZrO_2 calcined at 400 to 700 °C (acid ■; base □), or $NbWO_x/ZrO_2$ catalysts (acid ★; base ☆).

catalytic results of WO_3/ZrO_2 calcined at different temperatures (Fig. 6A). Nevertheless, there are optimal amounts of acid and base sites to obtain the maximum acrolein yield (Fig. 6B), which are 31–33 $\times$ 10^{18} sites per g catal for acidic sites and 7–12 $\times$ 10^{18} sites per g catal for basic sites. This is in consistence with the observation by Stošić *et al.*[30] that the selectivity of acrolein is largely governed by the balance between acidic and basic active sites. Fig. 6 also shows that when 1–5% Nb_2O_5 is doped in WO_3/ZrO_2-450, the acid amounts retain at relatively high values of 30–35 $\times$ 10^{18} sites per g catal, while the base amounts are shrunk in a narrower range of 7.5–8 $\times$ 10^{18} sites per g catal. Both are still in the range of the optimal amounts of acid and base sites to obtain the optimal acrolein yield.

In our case, most of the acidic sites on WO_3/ZrO_2-450 with and without doping Nb_2O_5 determined by pyridine adsorption are Lewis acid sites and the Brønsted acid sites are few and relatively weak. Therefore, Lewis acid sites seem to be the active sites for glycerol dehydration, and around 70% selectivities of acrolein are obtained. This finding is different from the literature reports that Lewis acids showed lower selectivities in the acrolein production than the materials containing Brønsted acids.[13] However, under the reaction condition where a large amount of water is present, it cannot be excluded that some Brønsted acidity may be generated through coordinative interaction of water molecules with Lewis acid sites on the catalysts. On the other hand, Kinage *et al.*[32] proposed that the basic sites were responsible for hydroxylacetone (HA) formation. Indeed, higher HA selectivities are obtained on the catalysts containing larger amounts of basic sites, such as WO_3/ZrO_2-400 and WO_3/ZrO_2-450 (Table 3).

As the decay rate is concerned, Fig. 6C shows that it decreases almost linearly with both amounts of acid and base sites, and those trends are in reverse to those of glycerol consumption rate. WO_3/ZrO_2-400 is the most stable catalyst among WO_3/ZrO_2 calcined at different temperatures (Fig. 3 and Table 3), while WO_3/ZrO_2-800 which contains lowest amounts of acid sites and almost no basic sites gives the lowest glycerol conversion, acrolein selectivity and faster decay rate. Since the acid sites, which are active for glycerol dehydration, are also active for coke formation, the fast decay rate observed over WO_3/ZrO_2-800 should be due to coking on the active sites. With the increasing amount of basic sites on WO_3/ZrO_2 catalysts, the decay rate slows down. Therefore, basic sites should contribute the suppression of coke formation.

For Nb-doped WO_3/ZrO_2-450, the product selectivities in 3–4 h TOS are almost unaffected upon Nb-doping, while the Unknowns selectivities decrease with decreasing the amount of basic sites. It has been proposed that too many basic sites would lead to formation of macromolecules, such as polyglycerols or acetalization products of glycerol.[33,34] Therefore, fine tuning the amount of basic sites is important. This conclusion is demonstrated in Fig. 6, in which the glycerol consumption rate, acrolein selectivity and catalyst decay rate all vary more drastically with the base amount than acid amount, and the optimal acrolein selectivity is obtained in a narrower range of base amount than that of acid amount.

Fig. S6 (ESI†) intends to correlate glycerol consumption rate, acrolein yield, and catalyst decay rate as a function of acid and base densities on the surface in the unit of sites per nm^2. No good correlation can be drawn, implying that the catalytic performance is less affected by the acid and base densities on the surface.

Fig. 7 correlates the catalytic performances with the ratio of acid/base sites. It shows the best performances are over Nb-doped WO_3/ZrO_2-450 catalysts which have acid/base ratios of 4.0–5.4. It is also noticed that there appears a narrow range of acid/base ratios of 3.25–3.5 giving lowest glycerol consumption rate, low acrolein yield, and fast catalyst decay rate. These results demonstrate again that fine tuning the ratio of acid/base sites is important in achieving good catalytic performance in gas-phase dehydration of glycerol to generate acrolein.

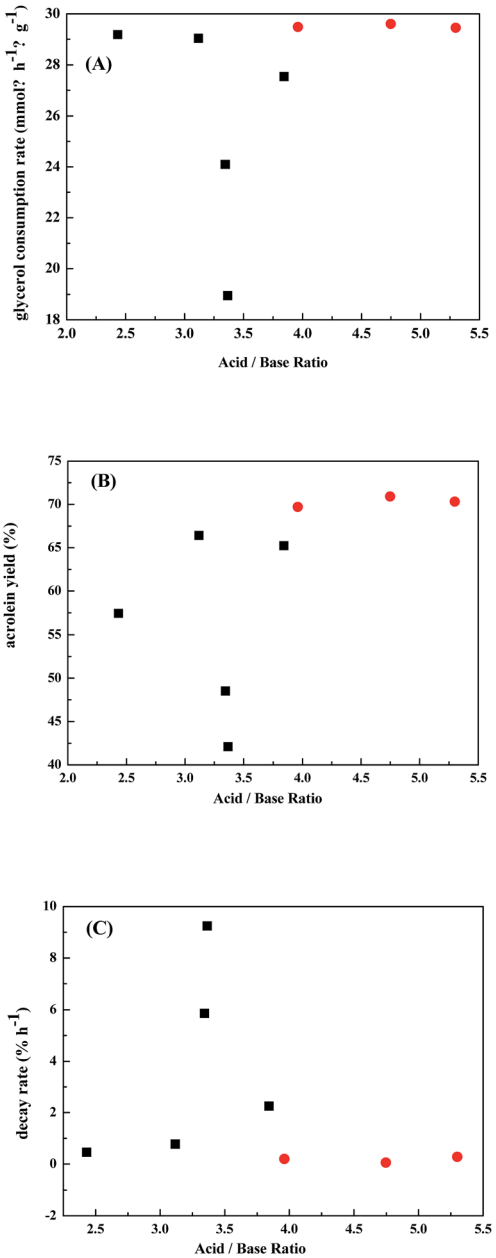

Fig. 7 Correlations of (A) specific glycerol consumption rates, (B) acrolein yields, and (C) decay rates (average in 3–12 h TOS) with acidic/basic ratios on WO_3/ZrO_2 calcined at 400 to 700 °C (■) or $NbWO_x/ZrO_2$ catalysts (●).

4. Conclusions

Total amounts of acid and base sites of WO_3/ZrO_2 catalysts prepared by impregnation method decreased with the increase of calcination temperature. In gas-phase dehydration of glycerol, the glycerol consumption rate increased almost linearly with total amounts of acid and base sites, while those calcined at 450–700 °C gave highest acrolein selectivities of 68–71%. Moreover, the decay rate of the catalysts slowed down with the increase of total amounts of acid and base sites. The most suitable calcination temperature for WO_3/ZrO_2 catalyst was 450 °C in consideration of high acrolein yield and long lifetime of the catalyst. Furthermore, the deactivation of the catalyst could be greatly improved by doping small amount of niobium. Most of the acidic sites on WO_3/ZrO_2-450 with and without doping Nb_2O_5 are Lewis acid sites and the Brønsted acid sites are few and relatively weak. The optimal catalytic performance was obtained over 3% $NbWO_x/ZrO_2$-450. The glycerol conversion was kept at 82% after 24 h. The improvement of catalyst is attributed to that basic sites on the ZrO_2 support are neutralized by niobium. The glycerol consumption rate increases almost linearly with both amounts of acid and base sites. Nevertheless, there are optimal amounts of acid and base sites to obtain the maximum acrolein yield. Fine tuning the ratio of acid/base sites is important in achieving good catalytic performance in gas-phase dehydration of glycerol to generate acrolein. High glycerol consumption rate, high acrolein yield, and slow catalyst decay rate are observed over Nb-doped WO_3/ZrO_2-450 catalysts which have acid/base ratios of 4.0–5.4. The spent catalysts could be easily regenerated by calcination at 450 °C for 3 h, and the catalytic activities were well retained.

Conflicts of interest

There are no conflicts to declare.

Acknowledgements

Financial supports from Ministry of Science & Technology, Taiwan (104-2119-M-002-019) are gratefully acknowledged.

Notes and references

1 L. C. Meher, D. Vidya Sagar and S. N. Naik, *Renewable Sustainable Energy Rev.*, 2006, **10**, 248–268.
2 F. Yang, M. A. Hanna and R. Sun, *Biotechnol. Biofuels*, 2012, **5**, 13.
3 B. Katryniok, S. Paul, M. Capron and F. Dumeignil, *ChemSusChem*, 2009, **2**, 719–730.
4 S. Kahlbaum, FR Patent No. 695931, 1930.
5 M. Watanabe, T. Iida, Y. Aizawa, T. M. Aida and H. Inomata, *Bioresour. Technol.*, 2007, **98**, 1285–1290.
6 H. Groll and G. Hearne, *US Pat.*, No. 2042224 1936.
7 H. Hoyt and T. Manninen, *US Pat.*, No. 2558520 1951.
8 A. Neher, T. Haas, A. Dietrich, H. Klenk and W. Girke, DE Patent No. 4238493, 1994.
9 E. Tsukuda, S. Sato, R. Takahashi and T. Sodesawa, *Catal. Commun.*, 2007, **8**, 1349–1353.
10 S.-H. Chai, H.-P. Wang, Y. Liang and B.-Q. Xu, *Appl. Catal., A*, 2009, **353**, 213–222.
11 J. L. Dubois, C. Duquenne and W. Hoelderich, WO 2006087083 2006.
12 J. L. Dubois, C. Duquenne, W. Hoelderich and J. Kervennal, WO 2006087084 2006.
13 S.-H. Chai, H.-P. Wang, Y. Liang and B.-Q. Xu, *Green Chem.*, 2007, **9**, 1130–1136.
14 A. Ulgen and W. F. Hoelderich, *Appl. Catal., A*, 2011, **400**, 34–38.
15 S.-H. Chai, H.-P. Wang, Y. Liang and B.-Q. Xu, *J. Catal.*, 2007, **250**, 342–349.
16 N. R. Shiju, D. R. Brown, K. Wilson and G. Rothenberg, *Top. Catal.*, 2010, **53**, 1217–1223.
17 M. Massa, A. Andersson, E. Finocchio and G. Busca, *J. Catal.*, 2013, **307**, 170–184.
18 Y. Y. Lee, K. A. Lee, N. C. Park and Y. C. Kim, *Catal. Today*, 2014, **232**, 114–118.
19 P. Lauriol-Garbey, J. M. M. Millet, S. Loridant, V. Bellière-Baca and P. Rey, *J. Catal.*, 2011, **281**, 362–370.
20 P. Lauriol-Garbey, G. Postole, S. Loridant, A. Auroux, V. Belliere-Baca, P. Rey and J. M. M. Millet, *Appl. Catal., B*, 2011, **106**, 94–102.
21 P. Lauriol-Garbey, S. Loridant, V. Bellière-Baca, P. Rey and J.-M. M. Millet, *Catal. Commun.*, 2011, **16**, 170–174.
22 R. Znaiguia, L. Brandhorst, N. Christin, V. Bellière Baca, P. Rey, J.-M. M. Millet and S. Loridant, *Microporous Mesoporous Mater.*, 2014, **196**, 97–103.
23 A. Ulgen and W. Hoelderich, *Catal. Lett.*, 2009, **131**, 122–128.
24 A. Martínez, G. Prieto, M. A. Arribas, P. Concepción and J. F. Sánchez-Royo, *J. Catal.*, 2007, **248**, 288–302.
25 C. García-Sancho, J. A. Cecilia, A. Moreno-Ruiz, J. M. Mérida-Robles, J. Santamaría-González, R. Moreno-Tost and P. Maireles-Torres, *Appl. Catal., B*, 2015, **179**, 139–149.
26 C.-J. Jia, Y. Liu, W. Schmidt, A.-H. Lu and F. Schüth, *J. Catal.*, 2010, **269**, 71–79.
27 M. Dalil, D. Carnevali, M. Edake, A. Auroux, J.-L. Dubois and G. S. Patience, *J. Mol. Catal. A: Chem.*, 2016, **421**, 146–155.
28 M. Dalil, M. Edake, C. Sudeau, J.-L. Dubois and G. S. Patience, *Appl. Catal., A*, 2016, **522**, 80–89.
29 M. Dalil, D. Carnevali, J.-L. Dubois and G. S. Patience, *Chem. Eng. J.*, 2015, **270**, 557–563.
30 D. Stošić, S. Bennici, J.-L. Couturier, J.-L. Dubois and A. Auroux, *Catal. Commun.*, 2012, **17**, 23–28.
31 J. H. Bitter, M. K. van der Lee, A. G. T. Slotboom, A. J. van Dillen and K. P. de Jong, *Catal. Lett.*, 2003, **89**, 139–142.
32 A. K. Kinage, P. P. Upare, P. Kasinathan, Y. K. Hwang and J.-S. Chang, *Catal. Commun.*, 2010, **11**, 620–623.
33 D. G. Barton, M. Shtein, R. D. Wilson, S. L. Soled and E. Iglesia, *J. Phys. Chem. B*, 1999, **103**, 630–640.
34 C. García-Sancho, R. Moreno-Tost, J. Mérida-Robles, J. Santamaría-González, A. Jiménez-López and P. Maireles-Torres, *Appl. Catal., A*, 2012, **433**, 179–187.